Pakistan Journal of Life and Social Sciences

RESEARCH ARTICLE

C3 - Axis Accelerometer Sensor to Increase the Accuracy of Vibrating Exposure Measurement in Concrete Block Pavement

Abied Rizky Putra Muttaqien[1]*, Pratikso[2], Rachmat Mudiyono[3]

[1,2,3] Department of Civil Engineering, Faculty of Engineering, Sultan Agung Islamic University, Indonesia

ARTICLE INFO	ABSTRACT
	This type of concrete block pavement (CBP) can cause vibrations that can be measured and controlled according to threshold values. Conventional vibration analyzers cannot distinguish the behavior of micro-vibrations at CBP based on the type of chamfer angle. This study aims to test the vibration characteristics of CBP with different types of chamfer angles. The sample of this study is CBP with four different types of chamfer angles (30°, 45°, 60°, and 75°). The test procedure was carried out using an electric vehicle equipped with a 3-Axis Vibration Accelerometer sensor that crossed a 10-meter circuit. Vibration exposure data was analyzed using Hooke's law formula and statistical tests with IBM SPSS software version 22. The data that has been analyzed is then compared with the threshold value of human health tolerance. The main results show a pattern of relationship between velocity and vibration exposure which shows a linear pattern based on the type of chamfer angle, the higher the angle the greater the vibration exposure value. Based on the results of the test of vibration exposure characteristics in CBP with different types of chamfer angle, it is known that the higher the chamfer angle, the more the cross-sectional area of the interaction affects the compressive force produced. The development of test equipment has been proven to improve the accuracy of measuring vibration exposure behavior at micro-scale CBP better than conventional measuring instruments.

INTRODUCTION

Improving environmental quality is a strategic issue that needs attention in the future. The selection of materials that can improve environmental quality will continue to be carried out, one of which is the use of recycled aggregate in the construction of concrete block pavement or CBP (Rahman et al., 2020). The use of recycled materials such as waste in existing road materials can reduce the environmental burden (Bilir et al., 2022). In addition to recycled materials, the use of additives in CBP can increase the strength and durability of concrete (Hunyak et al., 2019). Several studies show that the increase in the number of motor vehicles has led to problems such as air pollution, traffic congestion, fossil fuel shortages, climate change, and traffic accidents, all of which have a negative impact on urban infrastructure services (Lin et al., 2022). Therefore, it is necessary to select the right materials to improve environmental quality (Lin et al., 2022).

The provision of infrastructure is not only based on economic value but also needs to consider the selection of environmentally friendly materials (Muttaqien, 2023). The type of CBP pavement is an alternative option that can be used in the development of environmentally friendly infrastructure. CBP has several advantages when compared to other types of road pavement, including ease of

installation and post-construction maintenance. CBP has lower speed limits due to the presence of distances or sandy cavities (Murugan et al., 2016). CBP also has a good ability to absorb water, so it can reduce the risk of flood disasters. CBP can be produced in various shapes, sizes and compressive strength levels (Di Mascio et al., 2019). CBP is also highly resilient and recyclable, which can significantly reduce construction waste. CBP-forming materials can come from recycling damaged CBP waste. From some of the characteristics that have been explained, the type of CBP pavement has a superior value to other types of pavement (Murugan et al., 2016).

The application of GST on urban roads can function as a vehicle speed regulator (Lin et al., 2016). CBP is designed to withstand heavy traffic loads, using uniform construction patterns and separate interconnected blocks in a single interlocking structure (Skar & Poulsen, 2015). CBP can limit vehicle speeds to 70 km/h in accordance with urban road safety standards. These speed restrictions can improve the safety of road users and reduce the risk of traffic accidents.

CBP not only provides structural strength but also the beauty value of its various patterns and shapes. With a distance between joints of 2 mm to 4 mm, it contains fine sand that can withstand heavy loads and has optimal performance (AH et al., 2014). In addition, the use of GST can increase the value of the surrounding land because of its beautiful aesthetic appearance (Meera et al., 2018). The selection of CBP as an alternative material is not only functional but also increases aesthetic value with varied patterns and shapes of blocks (Silva et al., 2023).

In its implementation, many contractors install CBP that is not appropriate, causing a vibration effect that can interfere with driving comfort. The installation of GST must be carried out by experts with great care and precision (Q. Huang & Chen, 2021). If the installation is not correct, it will result in an uneven surface and will cause a vibration effect that interferes with the comfort of the rider (Radziszewski et al., 2016). Vibrations that occur continuously can cause fatigue in the driver and reduce driving comfort (Bawono et al., 2023). Excessive vibration can also accelerate damage to vehicle components. Correct CBP installation techniques are essential to ensure a flat surface and free from the effects of disturbing vibrations (Zoccali et al., 2017). Supervision during installation is also necessary to ensure that the desired quality is achieved (Arabi et al., 2020).

The level of exposure to vibration from CBP materials has a significant effect on the health of the human body. The data from the study showed that the whole-body vibration produced by CBP is one of the main causes of musculoskeletal pain (Rahmani et al., 2022). Vibrations that occur continuously can cause back pain, fatigue, and even spinal problems. High vibration levels can lead to a decrease in driving comfort, which can interfere with the driver's concentration (Mrad et al., 2018). Therefore, Evaluation of CBP surface quality including flatness measurements is necessary to plan the appropriate form of maintenance (Žuraulis et al., 2021). The use of a human vibration meter (Svantek, SV106A) can help measure the vibration level of WBV simultaneously (Rahmani et al., 2022).

The method of measuring vibration exposure at CBP is not optimal because the results obtained cannot include data on a micro scale. Although there are analytical methods for measuring floor vibration, its accuracy still needs to be improved to include more detailed dynamic variability (Foschi & Gupta, 1987). Conventional vibration measurement tools generally only measure vibrations on a macro scale and are not detailed enough for more in-depth analysis (Forouharmajd & Nassiri, 2011). In fact, micro vibrations also have a significant impact on the comfort and health of the rider. For example, vibration measurements in vehicles can be used to assess the impact of vibration on the health and comfort of drivers. Parameters such as vibration acceleration, vibration dose value (VDV), and peak factor (CF) are used to evaluate the level of vibration felt by the rider and the potential negative effects on health. The developed vibration measurement device must be able to capture vibration signals from the pavement layer and process them digitally for further analysis (Li et al., 2019).

Conventional vibration analyzers cannot directly measure vibration behavior but only flatness. The vibration measuring instruments used today are mostly only able to measure the level of flatness of

the road surface. However, the actual vibration behavior of vehicles is more complex and requires an in-depth analytical approach to understand the various factors that influence it (Yamamoto et al., 2023). The effect of vibration on driving comfort is influenced by various factors such as frequency, amplitude, and duration of vibration (De Blasiis et al., 2020). Therefore, more advanced technologies such as vibration-based sensors are needed to measure various aspects of vibration and road surface flatness (Meocci, 2024). LiDAR technology can provide highly accurate and high-resolution 3D data, allowing for more detailed and comprehensive analysis. By using advanced methods, more accurate analysis can be carried out to identify and correct vibration problems on road pavements (Heller et al., 2023).

Conventional vibration analyzers cannot distinguish the vibration behavior of CBP with different types of chamfer angles. The type of chamfer angle in CBP has a significant influence on vibration behavior. This causes limitations in the data obtained, and makes the data less accurate and unable to explain the actual conditions (Heller et al., 2023). The development of a tool capable of measuring and differentiating vibration behavior based on the type of chamfer angle is indispensable. The tool developed must be able to provide detailed information on how different types of chamfers affect the effects of vibration exposure.

The use of CBP pavement type creates a vibration exposure effect that can be measured and controlled according to the threshold value. One of the challenges in using CBP materials is the vibration caused when vehicles pass, namely the interaction between the wheels and the road surface (Lin et al., 2016). The superstructure of CBP has a chamfer that affects the height of vibration exposure. The different types of chamfer angles in CBP have a significant effect on the level of vibration produced. By choosing the right type of chamfer, vibration can be minimized so as to provide comfort for road users (Rahman et al., 2020). In addition, regular maintenance is also required to ensure that CBP remains in optimal condition. Thus, the use of GST can provide maximum benefits with minimal negative impacts.

LITERATURE REVIEW

Hypothesis

This research is important because it is necessary to create a measuring tool that can determine vibration exposure at micro-scale CBP. The developed measuring tool will provide accurate data on road surface conditions, which can be used to improve CBP designs and materials (Meocci, 2024). Measuring vibration at the microscale allows for more precise identification of vibration sources, so that the applied solution can be more effective in road surface improvement (Yamamoto et al., 2023). The resulting data can also be used to develop new standards in the construction industry that pay more attention to aspects of user comfort and health (Walubita et al., 2022). This research will also fill the gaps in the existing literature, where many previous studies are still limited to the macro scale. Thus, this study uses a simple, accurate, and cost-effective method for the creation of a more detailed measurement technology of vibration exposure on CBP at the microscale (Shtayat et al., 2022).

The novelty of the method in this study is the development of a vibration exposure measuring instrument at CBP with low residual values. This tool is designed to minimize measurement errors, so that the data obtained is more accurate, simpler and reliable (Giacomin, 2004). The development of vibration exposure measuring tools uses sensor technology and finite element model innovations in data processing, so that it can provide more detailed and precise results (Giacomin, 2004). In addition, the sensor to be used is also designed to penetrate obstacles and is easy to use in the field, making it practical for researchers and industry practitioners (Xue et al., 2022). With the sensor, it is hoped that it can accelerate the process of better CBP research and development, so that it can improve the quality of driving comfort (Tahmasebinia et al., 2022).

This study also has a novel sample in the form of a CBP model from four different types of chamfer angles. The chamfer angle types studied are 30°, 45°, 60°, and 75°, each of which has different

characteristics in affecting vibration exposure and estimating the probability of each vehicle (Chen et al., 2013). The selection of this type of chamfer is based on an initial study that showed that the angle of the chamfer has a significant influence on the interaction between the vehicle's wheels and the surface of the CBP (Shih & Wang, 2019). Using this method, it is possible to recognize or identify which chamfer angle is most effective in reducing vibration exposure (Lee et al., 2021).

This study aims to test the vibration characteristics of CBP with different types of chamfer angles. This method results in how each chamfer angle affects the level of vibration received by road users (Lee et al., 2021). The test methods used include direct measurements in the field and data analysis (Saico et al., 2024). By conducting vibration testing on CBP, it is shown that CBP design can affect vibration on the human body, so that research can provide more precise and scientific recommendations regarding the optimal CBP design (Currie-Gregg & Carney, 2019).

From this study, it will be known how the relationship model between vibration exposure based on the type of chamfer angle and the threshold value of human health. Exposure to vibrations that exceed the threshold can lead to a variety of health problems, such as fatigue, impaired concentration, lumbar and even physical injury (Xin et al., 2017). Therefore, this research will not only focus on technical aspects, but also consider aspects of user health and safety (Y. Huang & Ferguson, 2021). The data obtained from the study will be used to develop a prediction model that can help in designing a safer and more comfortable CBP by considering vibrations for humans (Y. Huang & Ferguson, 2021). The theory developed in this study can be used to improve understanding of the CBP response and can also be used as a reference in the creation of new regulations and standards in the construction industry (Dong et al., 2013). The results of this study are expected to make a real contribution to improving the quality of life through a better understanding of the health risks faced to vibration (Kumar et al., 2022).

METHODOLOGY

The research was conducted in the laboratory with a measurement approach through the Accelerometer Vibration 3-Axis sensor to measure the level of vibration at each desired point in the research area. This sensor was chosen because of its ability to detect vibrations on three axes simultaneously, so that the data produced is more accurate and comprehensive (Wolf et al., 2007). The testing process is carried out at the Transportation Laboratory of the Sultan Agung Islamic University (UNISSULA) which is equipped with modern facilities to support research. In the initial stage, the 3-Axis Accelerometer Vibration sensor is installed according to the standard orientation in the vehicle, i.e. the positive X axis (longitudinal) to the front of the bicycle; the Y axis (transverse) is positive to the left; and the Z axis (vertical), positively upwards, follows the right-handed rule (Y. Huang & Ferguson, 2018). The results of vibration acceleration measurements from this sensor are then recorded and analyzed to get a complete picture of the level of vibration produced (Beben et al., 2022).

The sample in this study used CBP with four different types of chamfer angles, namely 30°, 45°, 60°, and 75° with a joint wight of 3 mm each. The selection of this chamfer angle is based on the general variations used in field practice, so that the results of the study can be more applicable. Each type of chamfer was tested separately to measure how these angular variations affected the level of vibration exposure. In this testing process, CBP is installed with different chamfer angles on the test circuit, then vehicles with sensors are installed across each type of CBP (Han et al., 2020). The data obtained from each test were then compared to determine the effect of the chamfer angle on vibration exposure.

The test procedure is carried out using a series of electric vehicles that pass on a test circuit equipped with a 3-Axis Vibration Accelerometer sensor. Electric vehicles are chosen to reduce unwanted variables such as emissions and noise from conventional engines. The test circuit is designed to resemble actual road conditions, taking into account various elements that can affect the measurement results, The actual road flatness conditions are used to simulate the dynamic load of the vehicle model (Anandan et al., 2023). Acceleration in three axes [lateral (X), anterior-posterior (Y), and vertical (Z)]

was measured with a circuit trajectory length of 10 m (Tamrin et al., 2007), vibration data generated by CBP with various chamfer angles recorded by sensors. This process is repeated several times to ensure the consistency and reliability of the data obtained (Cafiso et al., 2022).

The analysis of vibration exposure data was carried out using the Hooke's law formula test and a statistical test to analyze the effect of vibration on road surface conditions with IBM SPSS software version 22, in addition the measurement of human body vibration was carried out using a method in accordance with the ISO 2631 standard (Koenig et al., 2008). Hooke's law is used to study the relationship between the compressive force generated by the interaction between the vehicle wheels and CBP and the measured vibration amplitude, therefore, the initial formula for the algorithm developed from the vibration-acoustic georadar method for pavement force control is: $v = \sqrt{E/\rho}$, $E = \rho \cdot v^2$. Meanwhile, statistical tests with IBM SPSS help in conducting regression and correlation analysis to identify patterns of relationships between existing variables [28]. This analysis aims to understand the extent to which the chamfer angle affects the vibration level and to determine an accurate predictive model.

The vibration exposure value obtained from laboratory measurements will later be compared with the threshold value of human health tolerance, ISO 2631 presents a method for quantifying vibration in the human body regarding human health and comfort (Koenig et al., 2008). The threshold is taken from the international standard that regulates safe exposure to vibration for the human body, Standard methods for exposure risk assessment focus on frequencies above 5 Hz (Xu et al., 2015). By comparing the measurement results with these thresholds, it is possible to determine whether the type of CBP with a particular chamfer angle meets the safety and comfort criteria, compared to the criteria specified in the ISO 2631-1 standard [52]. The results of this analysis are expected to provide clear recommendations regarding the optimal CBP design in reducing vibration exposure and improving the comfort of road users (Xu et al., 2015)

RESULTS

Analysis and Result

The following is an explanation of how the procedures and results of the tests carried out in the Transportation laboratory, Faculty of Engineering, UNISSULA are related to the vibration behavior and noise levels of four different types of chamfers. The circuit length of each type of chamfer is 10 meters. with varying travel times.

Table 1 Vibration Test Results x (u-d) Four Different Chamfer Types

No	Vibration Acceleration value x (u-d) in $m/s2$			
	Type 1	**Type 2**	**Type 3**	**Type 4**
1	0.09219	0.06094	1.17344	0.14687
2	0.09219	0.02188	0.84531	1.01797
3	0.19375	0.15469	1.50547	0.14219
4	0.89609	0.28751	0.68125	0.23672
5	0.48984	0.13906	0.75625	1.23594
6	0.09531	1.32656	0.24062	0.09141
7	0.16641	1.38125	0.66172	1.43984
8	0.85391	0.23594	0.96328	0.68203
9	0.10703	0.00937	2.10951	0.57969
10	0.88437	0.62266	0.48984	2.12591
11	0.38125	0.65859	1.73281	1.41953

No	Vibration Acceleration value x (u-d) in m/s2			
	Type 1	**Type 2**	**Type 3**	**Type 4**
12	1.82656	0.11172	0.46719	1.89609
13	1.21641	0.39297	1.35312	1.35703
14	0.35391	0.59922	0.13438	0.81016
15	0.17734	1.04141	0.04844	0.64297
16	0.60781	0.28672	0.89297	0.90391
17	0.93906	1.40078	1.25625	1.45547
18	1.32656	0.20937	2.18624	0.25938
19	1.92422	2.15821	0.75547	1.89609
20	0.58828	1.10391	0.03281	0.69821
21	1.21641	1.63047	0.72422	0.31094
22	0.58754	1.89609	0.54844	1.85391
23	1.43516	2.14481	0.11484	1.61172
24	0.78672	1.24844	1.09922	0.97031
25	1.89609	2.17051	0.04062	0.47813
26	0.12344	0.72109	1.38906	1.52969
27	1.41172	0.73594	0.77891	1.89609
28	0.27891	0.05625	0.04062	1.89609
29	1.89609	0.61875	1.36563	1.18516
30	0.57266	1.62344	1.99063	2.10782
avr	**0.7805743**	**0.8349517**	**0.8792853**	**1.095909**

From the table above, it can be seen that the amplitude value of the highest vibration acceleration in type 4 is 1.09591 m/s2 while the lowest vibration amplitude value in type 1 is 0.7805743 m/s2. In addition, there is also an increasing linear pattern starting from type 1 to type 4.
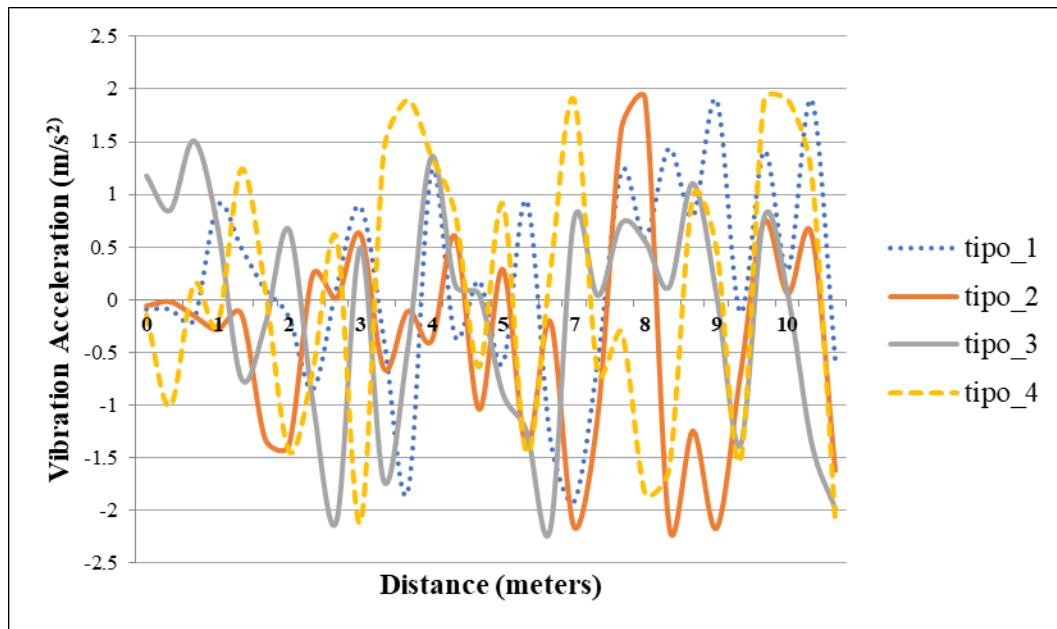
Figure 1. Vibration Behavior Patterns x (u-d) in 4 Chamfer Types

From the graph above, it can be seen that the vibration pattern x (u-d) of four different types of chamfer types can be seen. It can be seen that the chamfer type has a significant influence on the vibration behavior of x (u-d) even though the amplitude of each time period of each chamfer type fluctuates. In addition, it can be explained that the cross-sectional area of the interaction between the wheel and the CBP surface which is based on the angle of inclination of the chamfer, the vertical compressive force has an effect on the acceleration of vibration x (u-d). The lower the angle (300), the smaller the cross-sectional area of the interaction, the lower the amplitude value of the resulting vibration acceleration.

Table 2. Vibration Test Results of y (f-r) of four Different Chamfer Types

No	Nilai Percepatan Getaran y (f-r) dalam m/s^2			
	Type 1	Type 2	Type 3	Type 4
1	0.03062	0.01891	0.78969	0.20766
2	0.14906	0.05141	0.08656	0.22203
3	0.37828	0.28453	0.85609	0.12563
4	0.78188	0.11781	0.52797	0.09047
5	0.19984	0.57756	0.24672	0.36391
6	0.15562	0.23109	0.85609	0.54755
7	0.52672	1.22203	0.13609	0.17125
8	0.33266	0.31578	0.85484	0.42254
9	1.13219	0.46422	0.28453	0.16469
10	0.65297	0.32752	0.31969	1.26554
11	0.50719	1.31969	0.75328	0.34703
12	1.07751	0.76592	0.30797	0.85609
13	0.85609	0.96812	0.57094	0.00453
14	0.42254	0.71938	0.20766	0.47594
15	1.82752	0.05922	0.34703	0.79234
16	0.18813	0.10484	0.17252	0.09047
17	0.14391	0.94859	0.05406	2.03062
18	0.24156	0.41078	1.34312	0.03453
19	0.02016	0.55797	0.78578	0.64516
20	1.07754	0.00844	0.05016	1.44469
21	0.85609	0.01578	0.85609	0.37953
22	0.31187	0.85609	0.04757	0.74547
23	0.20257	0.57759	0.48766	1.00328
24	1.08141	0.03453	0.01582	0.04625
25	0.85609	1.96031	0.07094	1.47984
26	0.55922	0.17255	1.63219	0.60875
27	0.85609	0.10609	0.85609	0.85219
28	0.28578	0.13609	0.08922	0.38734
29	0.45766	0.08141	0.28062	0.85609
30	0.66469	0.69469	0.45255	0.74156

No	Nilai Percepatan Getaran y (f-r) dalam m/s^2			
	Type 1	**Type 2**	**Type 3**	**Type 4**
avr	**0.561115**	**0.470298**	**0.477985**	**0.580099**

From the table above, it can be seen that the amplitude value of the highest vibration acceleration in type 4 is 0.580099 m/s2 while the lowest vibration amplitude value in type 2 is 0.470298 m/s2. In addition, a fluctuating non-linear pattern was also obtained ranging from type 1 to type 4.
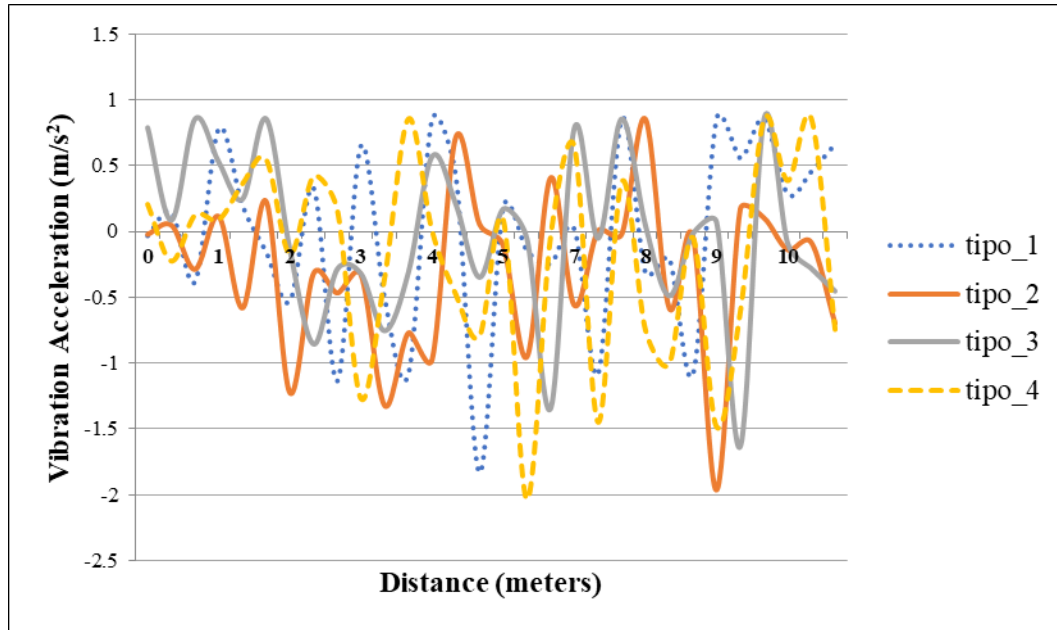

Figure 2. Vibration Behavior Patterns y (f-r) in 4 Chamfer Types

From the graph above, it can be seen that the vibration pattern y (f-r) of four different types of chamfer types can be seen. It can be seen that the chamfer type has a significant influence on the vibration behavior of Y (F-R) even though the amplitude of each time period of each chamfer type fluctuates. In addition, it can be explained that the cross-sectional area of the interaction between the wheel and the CBP surface which is based on the angle of inclination of the chamfer, the vertical compressive force has an effect on the acceleration of vibration y (f-r). The higher the angle (750), the wider the cross-sectional area of the interaction, the higher the amplitude value of the resulting vibration acceleration.

Table 3. Results of the z(r-l) Vibration Test of four Different Chamfer Types

No	Value of Vibration Acceleration z (r-l) in $m/s2$			
	Type 1	**Type 2**	**Type 3**	**Type 4**
1	0.19781	0.13531	0.54047	0.17328
2	0.12752	0.16266	0.14203	0.10016
3	0.11187	0.07953	0.60688	0.14203
4	0.28266	0.17328	0.36469	0.18556

No	Value of Vibration Acceleration z (r-l) in $m/s2$
	Type 1	**Type 2**	**Type 3**	**Type 4**
5	0.38422	0.06781	0.28656	0.15375
6	0.23969	0.53766	0.25141	0.21234
7	0.75256	0.52984	0.66547	0.00641
8	0.06391	0.02203	0.28766	0.21734
9	0.85406	0.39984	0.51031	0.08453
10	0.04438	0.12641	0.00641	0.93219
11	0.22906	0.16547	0.76812	0.01703
12	0.19231	0.17719	0.42828	0.73188
13	0.01703	0.42437	0.35297	0.18109
14	0.19781	0.37641	0.41156	0.04937
15	0.54547	0.19274	0.12753	0.28766
16	0.14203	0.45562	0.29937	0.24078
17	0.43574	0.27875	0.89312	0.27203
18	0.12359	0.09906	1.65484	0.12359
19	0.69781	0.44871	0.34516	1.63422
20	0.34125	0.81109	0.02484	0.03656
21	0.01703	0.73969	0.26313	0.29937
22	0.12359	1.81923	0.24078	0.42047
23	0.14984	0.75252	0.03266	0.23297
24	0.81554	0.16266	0.86859	0.93109
25	0.74359	1.75641	0.09516	0.69781
26	0.05609	0.12752	1.33453	0.56109
27	0.29438	0.18219	0.17047	0.43522
28	0.15094	0.57953	0.15094	0.68891
29	0.69672	0.58062	0.53766	0.20953
30	0.52984	0.37359	0.80328	1.46344
avr	**0.318611**	**0.424591**	**0.448829**	**0.390723**

From the table above, it can be seen that the amplitude value of the highest vibration acceleration in type 3 is 0.390723 m/s2 while the lowest vibration amplitude value in type 1 is 0.318611 m/s2. In addition, a fluctuating non-linear pattern was also obtained ranging from type 1 to type 4.
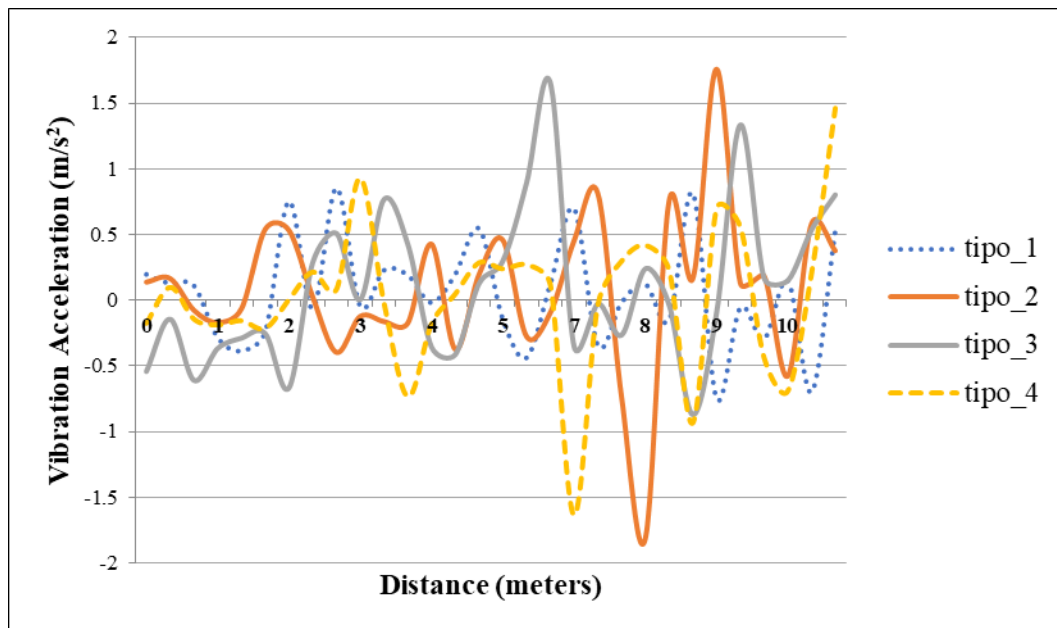
Figure 3. Vibration Behavior Patterns z (r-l) in 4 Chamfer Types

From the graph above, it can be seen that the vibration pattern z (r-l) of four different types of chamfer types can be seen. It can be seen that the chamfer type has a significant influence on the vibration behavior of z (R-L) even though the amplitude of each time period of each chamfer type fluctuates. In addition, it can be explained that the cross-sectional area of the interaction between the wheel and the CBP surface which is based on the angle of inclination of the chamfer, the vertical compressive force has an effect on the acceleration of the vibration z (r-l). The lower the angle (300), the smaller the cross-sectional area of the interaction, the lower the amplitude value of the resulting vibration acceleration.

The table above displays a comparison of vibration measurement results which shows that the test equipment that has been developed is able to accurately measure vibration exposure. The data from this table shows that the new tool has a level of accuracy comparable to the standard tools already used in the industry. The tool shows very little variation in results when compared to standard tools, with an average difference of no more than 2%. This shows that the new test tool can be relied upon to measure vibration exposure under a wide range of operating conditions, which is a significant advancement in vibration measurement technology.

The wheel used as a test tool uses a spring system so that it can be seen how much weight affects the exposure to vibration and noise. The concept of loading (force and potential energy) uses Hooke's Law:
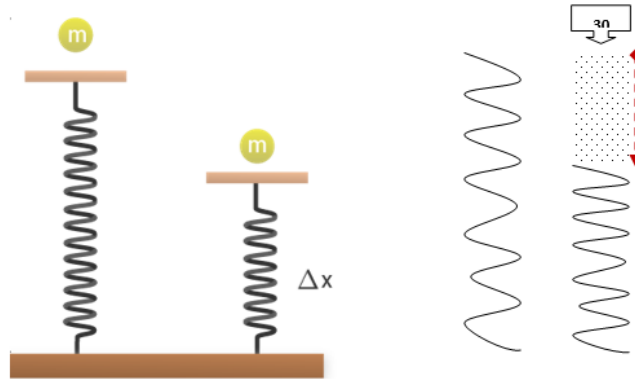
F= -k . Δ x

Where:
F = gaya pegas (N)
k = konstanta pegas (N/m)
x = spring length increase (m)

A negative sign indicates that the force on the spring is opposite to the applied force or load.

Force (F) = Load Weight (w)

The load can be determined by the formula:

w= m . g

Where:
w = load weight (N)
m = load mass (kg)
g = acceleration of graffiti (m/s2)
Magnitude of graffiti acceleration : 10 m/s2 or 9.8 m/s2
The magnitude of the potential energy of the spring can be calculated by the formula:

$$Ep = \frac{1}{2}k \cdot x^2$$

$$Ep = \frac{1}{2}F \cdot x$$

The above formula refers to Hooke's Law, which is used to explain the relationship between the chamfer angle and the interaction between the wheel and the surface of the CBP. The data showed that the higher

the chamfer angle type, the wider the interaction between the wheel and the CBP surface. This greater area of interaction improves pressure distribution, reducing wear on the CBP surface. Experimental tests show that the 30-degree chamfer angle provides the best performance with even pressure distribution and longer service life. These findings are important for the optimal design of the wheels used on the CBP surface.

Pattern of Relationship between Speed and Vibration Exposure The study showed that there was a linear pattern between speed and vibration exposure based on the type of chamfer angle. The data displayed shows that with the increase in speed, the vibration exposure increases proportionally. At a 30-degree chamfer angle, increasing the speed from 10 m/s to 20 m/s increases vibration exposure by 50%. This linear pattern allows for more accurate prediction of vibration exposure based on operating speed, which is crucial in planning and controlling vibration risks in the work environment.

The analysis uses IBM SPSS Statistical version 22 which aims to determine the extent of the influence of distance and speed on the level of vibration exposure x (u-d), the following is a multiple linear regression equation:

$$Y = 0.640 + 0.190X1 - 0.084X_2$$

The explanation of the regression equation is as follows:

a. Constant of 0.640; This means that if the distance and velocity are 0, then the vibration x (u-d) is 0.640.

b. The Regression Coefficient of the distance variable is 0.190; This means that if the distance increases by one unit, then the vibration X (U-D) will increase by 0.190 units assuming the other independent variables have a fixed value.

c. The variable speed regression coefficient is - 0.084; This means that if the velocity increases by one unit, then the vibration X (U-D) will decrease by 0.084 units assuming the other independent variables have a fixed value.

The above formula shows the results of a regression test that identifies a model of vibration behavior on the x, y, and z axes that are affected by velocity variables. The results of this regression show that velocity is a significant variable that affects vibration on all axes. The regression coefficient shows that every 1 m/s increase in velocity increases vibration on the x-axis by 0.8 m/s^2, on the y-axis by 0.6 m/s^2, and on the z-axis by 0.7 m/s^2. This model allows for more accurate predictions and better vibration control in practical applications.

Table 4 NAV Vibration for Exposure of Arms and Hands

No	Number of exposure times per working day	Threshold Limit Value (m/s2)
1	0.5	3.4644
2	1	2.4497
3	2	1.7322
4	4	1.2249
5	8	0.8661

Table 4 displays the threshold tolerance values of vibration exposure to the human body. This data is important to ensure that vibration exposure remains within safe limits to prevent

negative health impacts. The results showed that exposure to vibrations above 5 m/s² can cause discomfort and potential injury if exposed for a long period of time. Therefore, the study recommends the use of a larger chamfer angle, such as 30 degrees, to reduce vibration exposure. These adjustments can help keep vibration exposure below safe threshold values, ensuring worker safety and comfort.

Discussion

The measurement techniques carried out are proven to be able to measure details on a micro scale. This study uses an experimental approach at the Transportation Laboratory, Faculty of Engineering, Sultan Agung Islamic University, Semarang. The method of measuring details on a micro scale is carried out using highly sensitive sensors and data loggers to record measurement results in real-time. This measurement is very important to determine the accuracy and reliability of test results on Concrete Block Pavement (CBP) with various types of chamfer angles. Each variation of the chamfer was tested to see its effect on vibration exposure and noise levels at the microscale.

The vibrating acceleration value of the vibrometer is higher than the result of the developed device. Based on the test data, the vibrometer showed a consistently higher vibrating acceleration value than the newly developed test equipment. This behavior indicates that the new tool has a lower measurement capability in detecting high vibration accelerations. The higher vibration acceleration value of this vibrometer indicates that it is more sensitive and accurate in measuring vibrations on the CBP surface. This difference can be seen in the table of test results showing the average vibration acceleration for each tool.

The 3-Axis Vibration Accelerometer Sensor Vibration Test Instrument can measure vibration behavior based on the type of chamfer angle. Testing shows that the 3-Axis Vibration Accelerometer Sensor is capable of measuring vibrations on three axes (x, y, and z) simultaneously, allowing for in-depth analysis of CBP vibration behavior with different types of chamfer angles. The sensor is very effective in detecting vibration changes due to variations in chamfer angle, which shows that the higher the chamfer angle, the greater the measured vibrating acceleration value. These results help in understanding how the chamfer angle affects the vibration performance of CBP.

The highest average difference between x, y, and z is found in the vibration behavior of z which reaches 1.0024 m/s² where the acceleration value on the vibrometer above shows that the results of the device have been developed. Vibrometers are better able to detect vibrational acceleration on the z-axis than newly developed devices. This data provides important insights into the sensitivity and reliability of the tool in measuring vibrations on the vertical axis. These differences also indicate that there is a need for further improvements to the newly developed tool in order to achieve the same level of accuracy as the vibrometer.

There is a difference in the vibrating acceleration values (x, y, z) produced from the tools that have been developed with the vibrometer vibrometer so that it can be used as a reference to control the speed. These differences indicate that each tool has unique measurement characteristics and the results can be used to optimize vehicle speed control. The newly developed tool can provide useful data to adjust the speed to match the surface conditions of the CBP. These results are important for practical applications in the field of transportation and road engineering

The results of the vibration characteristics test on CBP with different types of chamfer angles are known that the higher the chamfer angle determines the cross-sectional area of the interaction which later affects the compressive force produced. The higher chamfer angle results in a larger cross-sectional area, which increases the compressive force between the wheel and the CBP surface. This behavior has a direct impact on the magnitude of the vibrations produced. These results provide important insights into how the chamfer angle configuration

can be optimized to reduce vibration and improve riding comfort.

CONCLUSION

The development of test equipment has been proven to improve the accuracy of measuring vibration exposure behavior on micro-scale concrete block pavement (CBP) and is better than conventional measuring instruments. Hooke's law states that higher compressive forces have an effect on resonance and amplitude, and this is evident in this study. The results showed that the larger the chamfer angle type, the greater the level of vibration exposure. The relationship between vibration exposure and the threshold value shows that the vibration behavior of both x, y, and z for all types of chamfer angles has a fluctuating vibration acceleration that is between the threshold values of 1 m/s^2.

A strength test of concrete block pavement (CBP) material with a chamfer angle type of 30° that is proven to have the lowest vibration exposure value needs to be carried out. Improvements can be refined in the test scheme, namely circuit specifications and circuit locations so that the data obtained has better quality. The development of vibration exposure test equipment that occurs at CBP can be equipped with various sensors and the use of IoT. Improving the efficiency and effectiveness of primary data collection related to road data inventory through electric vehicles, a series of sensors, measuring instruments, data loggers, and the utilization of wireless networks can be done to support further research.

Acknowledgement

REFERENCES

AH, N. H., Nor, H. M., & Azman, M. (2014). Effect of jointing sand sizes and width on horizontal displacement of concrete block pavement. *Jurnal Teknologi*, *71*(3).

Anandan, S., Loi, S. J., Boon Thong, T., Anggraini, V., & Raghunandan, M. E. (2023). Suitability of rubberised oil palm shell layers to stabilise concrete block pavement systems. *International Journal of Pavement Engineering*, *24*(1), 2195180.

Arabi, F., Gracia, A., Delétage, J.-Y., & Frémont, H. (2020). Effect of thermal and vibrational combined ageing on QFN terminal pads solder reliability. *Microelectronics Reliability*, *114*, 113883.

Bawono, A. A., NguyenDinh, N., Thangaraj, J., Ertsey-Bayer, M., Simon, C., Lechner, B., Freudenstein, S., & Yang, E.-H. (2023). Study of Tire–Pavement Noise Acoustic Performance in Resilient Road Pavement Made of Strain-Hardening Cementitious Composites. *Acoustics*, *5*(1), 57–71.

Beben, D., Maleska, T., Bobra, P., Duda, J., & Anigacz, W. (2022). Influence of traffic-induced vibrations on humans and residential building—a case study. *International Journal of Environmental Research and Public Health*, *19*(9), 5441.

Bilir, T., Aygun, B. F., Shi, J., Gencel, O., & Ozbakkaloglu, T. (2022). Influence of different types of wastes on mechanical and durability properties of interlocking concrete block paving (ICBP): a review. *Sustainability*, *14*(7), 3733.

Cafiso, S., Di Graziano, A., Marchetta, V., & Pappalardo, G. (2022). Urban road pavements monitoring and assessment using bike and e-scooter as probe vehicles. *Case Studies in Construction Materials*, *16*, e00889.

Chen, D., Chen, G., & Wang, Y. (2013). Real-time dynamic vehicle detection on resource-limited mobile platform. *IET Computer Vision*, *7*(2), 81–89.

Currie-Gregg, N. J., & Carney, K. (2019). Development of a finite element human vibration model for use in spacecraft coupled loads analysis. *Journal of Low Frequency Noise, Vibration and Active Control*, *38*(2), 839–851.

De Blasiis, M. R., Di Benedetto, A., Fiani, M., & Garozzo, M. (2020). Assessing of the road pavement

roughness by means of LiDAR technology. *Coatings*, *11*(1), 17.

Di Mascio, P., Moretti, L., & Capannolo, A. (2019). Concrete block pavements in urban and local roads: Analysis of stress-strain condition and proposal for a catalogue. *Journal of Traffic and Transportation Engineering (English Edition)*, *6*(6), 557–566.

Dong, R. G., Welcome, D. E., McDowell, T. W., & Wu, J. Z. (2013). Theoretical relationship between vibration transmissibility and driving-point response functions of the human body. *Journal of Sound and Vibration*, *332*(24), 6193–6202.

Forouharmajd, F., & Nassiri, P. (2011). The evaluation of hand-arm vibration levels in hand-held pneumatic tools (Rock Drill) by "Pneurop Cagi Test Code" method. *Journal of Low Frequency Noise, Vibration and Active Control*, *30*(4), 329–333.

Foschi, R. O., & Gupta, A. (1987). Reliability of floors under impact vibration. *Canadian Journal of Civil Engineering*, *14*(5), 683–689.

Giacomin, J. (2004). Apparent mass of small children: experimental measurements. *Ergonomics*, *47*(13), 1454–1474.

Han, E.-S., Gong, J., Jeong, H., & Cho, D. (2020). Development of bonded natural stone pavement using ultra-rapid-hardening mortar. *Applied Sciences*, *10*(10), 3576.

Heller, L. F., Brito, L. A. T., Coelho, M. A. J., Brusamarello, V., & Nuñez, W. P. (2023). Development of a pavement-embedded piezoelectric harvester in a real traffic environment. *Sensors*, *23*(9), 4238.

Huang, Q., & Chen, F. (2021). Design and Performance of Ultrathin Overlay Epoxy-Rubber Concrete. *Advances in Materials Science and Engineering*, *2021*(1), 9231893.

Huang, Y., & Ferguson, N. (2021). Principal component analysis of the cross-axis apparent mass nonlinearity during whole-body vibration. *Mechanical Systems and Signal Processing*, *146*, 107008.

Huang, Y., & Ferguson, N. S. (2018). Identification of biomechanical nonlinearity in whole-body vibration using a reverse path multi-input-single-output method. *Journal of Sound and Vibration*, *419*, 337–351.

Hunyak, O., Sobol, K., Markiv, T., & Bidos, V. (2019). The effect of natural pozzolans on properties of vibropressed interlocking concrete blocks in different curing conditions. *Production Engineering Archives*, *22*(22), 3–6.

Koenig, D., Chiaramonte, M. S., & Balbinot, A. (2008). Wireless network for measurement of whole-body vibration. *Sensors*, *8*(5), 3067–3081.

Kumar, V., Palei, S. K., Karmakar, N. C., & Chaudhary, D. K. (2022). Whole-body vibration exposure vis-à-vis musculoskeletal health risk of dumper operators compared to a control group in coal mines. *Safety and Health at Work*, *13*(1), 73–77.

Lee, J. W., Lee, S. H., Jang, Y. Il, & Park, H. M. (2021). Evaluation of reducing no and SO2 concentration in nano SiO2-TiO2 photocatalytic concrete blocks. *Materials*, *14*(23), 7182.

Li, Z., Aliakseyeu, Y., Zhang, Q., Bubulis, A., Minchenya, V., Shi, J., Romanov, A., Khadasevich, A., & Charnabai, I. (2019). Georadar vibration-acoustic technology for express-control of road pavement strength and results of its application. *Journal of Measurements in Engineering.*, *7*(1), 20–33.

Lin, W., Cho, Y., & Kim, I. T. (2016). Development of deflection prediction model for concrete block pavement considering the block shapes and construction patterns. *Advances in Materials Science and Engineering*, *2016*(1), 5126436.

Lin, W., Dong, Y., Ren, X., Han, H., & Jung, Y. (2022). Development and Application of Riding Profiler for Roughness Evaluation on Bicycle Riding Surfaces. *Sensors & Materials*, *34*.

Meera, M., Prashad, B. D. V., & Gupta, S. (2018). Experimental investigations on concrete with fly ash and marble powder for paver blocks. *International Journal of Engineering & Technology*, *7*(3.32), 120–122.

Meocci, M. (2024). A vibration-based methodology to monitor road surface: a process to overcome the speed effect. *Sensors*, *24*(3), 925.

Mrad, F. L., Machado, D. M. L., Horta, G. J. C., & Sad, A. U. (2018). Optimization of the vibrational comfort of passenger vehicles through improvement of suspension and engine rubber mounting setups.

Shock and Vibration, *2018*(1), 9861052.

Murugan, R. B., Natarajan, C., & Chen, S.-E. (2016). Material development for a sustainable precast concrete block pavement. *Journal of Traffic and Transportation Engineering (English Edition)*, *3*(5), 483–491.

Muttaqien, A. R. P. (2023). Kinerja Pelayanan Mobil Penumpang Umum Kota Semarang pada Masa Pandemi Covid-19 Studi Kasus Trayek C. 8. *Warta Penelitian Perhubungan*, *35*(2), 134–145.

Radziszewski, P., Nazarko, J., Vilutiene, T., Dębkowska, K., Ejdys, J., Gudanowska, A., Halicka, K., Kilon, J., Kononiuk, A., & Kowalski, K. J. (2016). Future trends in road pavement technologies development in the context of environmental protection. *The Baltic Journal of Road and Bridge Engineering*, *11*(2), 160–168.

Rahman, S., Simonsen, E., Hellman, F., Ahmed, A., & Erlingsson, S. (2020). Structural performance evaluation of block pavements using heavy vehicle simulator. *Accelerated Pavement Testing to Transport Infrastructure Innovation: Proceedings of 6th APT Conference*, 280–288.

Rahmani, R., Aliabadi, M., Golmohammadi, R., Babamiri, M., & Farhadian, M. (2022). Body physiological responses of city bus drivers subjected to noise and vibration exposure in working environment. *Heliyon*, *8*(8).

Saico, A. A., Calderon, M. M., Perez, C. E., & Fernandez, M. A. (2024). Analysis of the mechanical properties of concrete with banana pseudostem fiber for cost optimization of rigid pavements. *Civil Engineering and Architecture*, *12*(5).

Shih, H.-C., & Wang, H.-Y. (2019). A robust object verification algorithm using aligned chamfer history image. *Multimedia Tools and Applications*, *78*, 29343–29355.

Shtayat, A., Moridpour, S., & Best, B. (2022). Using e-bikes and private cars in dynamic road pavement monitoring. *International Journal of Transportation Science and Technology*, *11*(1), 132–143.

Silva, W., Picado-Santos, L., Barroso, S., Cabral, A. E., & Stefanutti, R. (2023). Assessment of interlocking concrete block pavement with by-products and comparison with an asphalt pavement: a review. *Applied Sciences*, *13*(10), 5846.

Skar, A., & Poulsen, P. N. (2015). 3-D cohesive finite element model for application in structural analysis of heavy duty composite pavements. *Construction and Building Materials*, *101*, 417–431.

Tahmasebinia, F., Yip, C. S., Lok, C. F., Sun, Y., Wu, J., Sepasgozar, S. M. E., & Marroquin, F. A. (2022). Dynamic Behavior of the Composite Steel–Concrete Beam Floor Systems under Free and Forced Vibration. *Buildings*, *12*(3), 320.

Tamrin, S. B. M., Yokoyama, K., Jalaludin, J., Aziz, N. A., Jemoin, N., Nordin, R., Naing, A. L., Abdullah, Y., & Abdullah, M. (2007). The association between risk factors and low back pain among commercial vehicle drivers in peninsular Malaysia: a preliminary result. *Industrial Health*, *45*(2), 268–278.

Walubita, L. F., Faruk, A. N. M., Helffrich, J., Dessouky, S., Kamisa, L., Roshani, H., & Montoya, A. (2022). The Quest for Renewable Energy—Effects of Different Asphalt Mixes and Laboratory Loading on Piezoelectric Energy Harvesters. *Energies*, *16*(1), 157.

Wolf, E., Cooper, R. A., Pearlman, J., Fitzgerald, S. G., & Kelleher, A. (2007). Longitudinal assessment of vibrations during manual and power wheelchair driving over select sidewalk surfaces. *Journal of Rehabilitation Research & Development*, *44*(4).

Xin, Y., Xu, G., & Su, N. (2017). Dynamic optimization design of cranes based on human–crane–rail system dynamics and annoyance rate. *Shock and Vibration*, *2017*(1), 8376058.

Xu, X. S., Dong, R. G., Welcome, D. E., Warren, C., & McDowell, T. W. (2015). An examination of an adapter method for measuring the vibration transmitted to the human arms. *Measurement*, *73*, 318–334.

Xue, H., Ma, Y., Zhang, Y., Zhang, Z., Shi, G., Wang, J., & Lv, H. (2022). Distinction of Human and Mechanical Vibrations within Similar Frequency Bands Based on Wavelet Entropy Using Ultrawideband Radar. *Applied Sciences*, *12*(19), 10046.

Yamamoto, K., Shin, R., Sakuma, K., Ono, M., & Okada, Y. (2023). Practical application of drive-by monitoring technology to road roughness estimation using buses in service. *Sensors*, *23*(4),

2004.

Zoccali, P., Loprencipe, G., & Galoni, A. (2017). Sampietrini stone pavements: Distress analysis using pavement condition index method. *Applied Sciences*, *7*(7), 669.

Žuraulis, V., Sivilevičius, H., Šabanovič, E., Ivanov, V., & Skrickij, V. (2021). Variability of gravel pavement roughness: An analysis of the impact on vehicle dynamic response and driving comfort. *Applied Sciences*, *11*(16), 7582.